Energy dependent optical potential for reactions involving ^{6,7}Li projectiles

V. A. B. Zagatto ⊙,[*] B. R. Gonçalves ⊙, and D. R. Mendes Junior ⊙

Instituto de Física da Universidade Federal Fluminense, 24210-346, Niterói, Brazil

The dependence of the optical Cook potential on the bombarding energies of reactions involving ^{6,7}Li projectiles has been analyzed. It has been found that, for reactions occurring close to or below the Coulomb barrier, the depth of the imaginary potential should be reduced from the value originally proposed by Cook in order to achieve better agreement with experimental elastic data. A modified version of the Cook potential is presented for both lithium isotopes, and its results are compared with those obtained using other existing optical potentials. Finally, the effects of the corrections made to the original Cook potential are studied in a one-neutron transfer case, highlighting the importance of using the correct optical potential for different reaction channels.

I. INTRODUCTION

To properly understand the evolution of our universe from the beginning until the present day, it is mandatory to determine the abundance of isotopes created during primordial nucleosynthesis. The hydrogen, helium, and lithium isotopes created during this process have given rise to a long chain of nuclear reactions occurring in various spatial environments, resulting in all of the nuclei observed today. However, a discrepancy still exists between experimental abundance observations and the theory for the ^{6}Li and ^{7}Li isotopes, as noted by [1]. Understanding the mechanisms that these nuclei undergo may shed some light on this problem.

Concerning to the case of lithium isotopes, the proper comprehension of such mechanisms is even more difficult since these nuclei may undergo the break-up (BU) process, breaking into an α particle plus a valence particle (^{2}H for ^{6}Li and ^{3}H for ^{7}Li). The possibility of breaking up opens a series of new reaction mechanisms which are not observed in other nuclei, such as the incomplete fusion process [2,3], where just one of the remaining fragments of the fragmented lithium is fused with the target while the other is scattered.

Since the nuclear mechanisms of reactions that may occur when lithium isotopes are involved are different from those observed in other nuclei, it is expected that the theoretical approach required to describe the reactions involving these isotopes may also be different. Some well-known examples are the continuum discretized coupled channels (CDCC) approach [4–8], the adiabatic approximation [9], and Faddeev-AGS equations [10]. While these methods deal with different aspects related to the reaction mechanisms that the lithium isotopes may undergo, they all share the common feature that their calculations are not easily implemented and are computationally consuming, demanding a high computational power. It is also well known that the BU mechanism may

have some influence on other reaction channels, such as fusion (making a separation between complete and incomplete fusion) [11] and elastic scattering.

As one may observe, a complete description of the BU mechanism is extremely difficult, making it quite attractive to perform calculations using an optical model approach that requires low computational power and depends on a few parameters. Besides, such simple calculations are useful from an experimental point of view, making possible to obtain reliable estimates of expected cross sections, allowing proper planning of experiments.

Due to their importance in the astrophysical scenario and the aforementioned difficulty in describing the reaction mechanisms that lithium isotopes may undergo, it is natural to expect that they have been widely studied and several optical potentials have been developed over the years trying to provide a good description of experimental data. Two recent examples of such potentials are found in Refs. [12,13], which were developed based on the analysis of a large existing database of elastic scattering. Among the existing optical potentials for ^{6,7}Li projectiles, the one developed by Cook [14] is one of the most commonly used until now. Cook developed an optical potential obtained from almost 70 elastic scattering data sets. The final potential was represented by a Woods-Saxon (WS) shape composed by a real and imaginary parts, with all parameters fixed except the depth of the imaginary part. This potential has a dependence based solely on the atomic mass of the target, making it quite easy and accessible for most users. The author did not find any dependence on the reaction energy, however, it should be noted that most of the data used to study the original potential were based on bombarding energies much above the Coulomb barrier. Therefore, the main aim of the present work is to reanalyze this energy dependence from the perspective of new data acquired since then. Such study is important because some reaction mechanisms, like the breakup reaction (BU), do not participate equally at all reaction energies. For instance, in Ref. [15], it was found that the coupling of the BU effect to

elastic channel calculations had a much greater impact when the reaction energy was around the Coulomb barrier. Since it is well established that ^{6,7}Li may undergo such effect, a new analysis mainly centered in this energy range makes sense. Therefore, the nuclear systems used in the present analysis will only be those for which data on elastic scattering under the Coulomb barrier are available. This should not be seen as a weak point of the present work since the region above the barrier has already been well studied by the original work of Cook, being unnecessary to revisit studies at this bombarding energy. From now on, the optical potential resulting from the systematics described in [14] will be referred to as the Cook potential.

Many recent works have successfully employed the Cook potential to study a variety of aspects of nuclear reactions. For instance, the elastic scattering of the ^{6}Li + ^{12}C reaction [16] has been analyzed using the Cook potential. In Ref. [17], the inelastic scattering of the ^{6}Li + ^{144}Sm [18] reaction has been studied, and it was found that the coupling of inelastic channels of the target were weakly coupled to the elastic scattering. Furthermore, the same reference also discusses another use of the Cook potential by using the results obtained from optical model calculations as a guide for the development of new reaction theories. Reference [19] uses the Cook potential to describe the breakup of the unstable isotope ^{8}Li. The use of the Cook potential to study transfer reactions has been employed in the ^{7}Li + ^{124}Sn reaction [20]. Finally, the use of the Cook optical potential to study complete and incomplete fusion in various reactions has been used in Refs. [21,22]. All of these examples demonstrate that the use of the Cook potential is still important and is widely used in recent works that aim to elucidate even more fundamental and microscopic aspects of nuclear reaction mechanisms.

The work is organized as follows. In Sec. II, the data selection and the data reduction performed is explained. Section III and its subsections bring the obtained results for ^{6}Li and ^{7}Li nuclei, as well as their comparison to the original Cook potential and other optical potentials existing in the literature. Finally, the application of the energy corrected Cook potential and its impact in the study of the one neutron transfer process is presented in this same section. The conclusions are presented in Sec. IV.

II. DATA SELECTION AND DATA REDUCTION

Before properly studying the possible effect of energy dependence on the Cook potential, it was necessary to select data for such a study. It is desirable that the selected elastic scattering angular distributions data have been measured with targets of different atomic masses, ranging from light to heavy nuclei. Additionally, the bombarding energy of ^{6,7}Li projectiles should be distributed in a region from below to above the Coulomb barrier of each nuclear reaction. This is particularly important because the Cook potential has been widely employed and used with several kinds of target nuclei of various atomic masses, and has proven to work well in most situations. It is also important to note that the Cook potential has been obtained mainly using data in the region above the Coulomb barrier. Therefore, the aim of the present work is to study the reactions occurring at energies around (and mainly below) the barrier.

To select the data, a search was carried out on the Ex-for database [23], selecting existing elastic data of reactions ranging from energies below the Coulomb barrier to over it. Since the number of measurements below the barrier is not very large and many measurements have been performed just over the barrier, many systems have not been considered in our analysis.

For the ^{6}Li projectile, reactions with ^{12}C, ^{27}Al, ^{28}Si, ^{58}Ni, ^{59}Co, ^{64}Zn, ^{90}Zr, ^{112,116,120}Sn, ^{208}Pb, and ^{209}Bi targets have been considered. In the case of ^{7}Li projectile, reactions with the ^{12}C, ^{27}Al, ^{28}Si, ^{59}Co, ^{64}Zn, ^{116,120}Sn, and ^{138}Ba isotopes have been considered. In total, 81 angular distributions have been analyzed to study the energy dependence of the Cook potential for ^{6}Li projectile, while 62 angular distributions have been considered for the same study for ^{7}Li nucleus. The list of used data is displayed in Table I. The Coulomb barrier has been calculated using the well-known semiempirical formula $E_{\mathrm{c.m.}}^{\mathrm{barr}} = \frac{0.9Z_1Z_2}{A_1^{1/3}+A_2^{1/3}}$ [24], where Z_i and A_i are the atomic and mass numbers of each participating nucleus. One may notice from Table I that most of the references have been acquired after the publication of the original work of [14].

The systematic approach used in the present work consisted of verifying the energy dependence of the imaginary part of the optical potential developed by Cook [14]. Therefore, all the parameters previously found in Cook's work are still valid for ^{6}Li and ^{7}Li. For both nuclei, a Coulomb radius of $R_{\mathrm{Coul}} = 1.3$ fm should be used. When using a ^{6}Li projectile, one should adopt the following parameters for a complex Woods-Saxon shape of the optical potential:

$$V_R = 109.5 \text{ MeV}, \quad r_R = 1.326 \text{ fm}, \quad a_R = 0.811 \text{ fm},$$
$$r_I = 1.534 \text{ fm}, \quad a_I = 0.884 \text{ fm}, \tag{1}$$
$$W_I = 58.16 - 0.328\,A + 0.00075\,A^2 \text{ MeV}.$$

One may notice from Eq. (1) that all the parameters are fixed, except by the imaginary depth of the potential, which depends on the mass of the target nucleus. A similar form is observed in the complex potential of ^{7}Li projectile, which may be visualized in Eq. (2) (once again adopting $R_{\mathrm{Coul}} = 1.3$ fm):

$$V_R = 114.2 \text{ MeV}, \quad r_R = 1.286 \text{ fm}, \quad a_R = 0.853 \text{ fm},$$
$$r_I = 1.739 \text{ fm}, \quad a_I = 0.809 \text{ fm}, \tag{2}$$
$$W_I = 40.13 - 0.341\,A + 0.00093\,A^2 \text{ MeV}.$$

The parameters used in Eqs. (1) and (2) are simply those originally proposed in [14]. After selecting this data, we found the best fit between elastic scattering data and theoretical calculations. The calculations used the V_R, $r_{R,I}$, and $a_{R,I}$ values proposed in Eqs. (1) and (2), just allowing the variation of the depth of the imaginary potential. The best fit was found by the reduction of the χ^2 value using the code SFRESCO [25]. We visually verified the comparison between data and the found adjustment one by one. This was necessary because some data had no error bars for some data points (typically for the most frontal ones), so the best fit obtained might give a lot of weight to these specific data points, resulting in a tendency

TABLE I. Table displaying the Coulomb barrier, bombarding energies, and references for each combination of projectile-target analyzed in this work.

Projectile	Target	$E_{\text{lab}}^{\text{barr}}$ (MeV)	E_{lab} (MeV)	References
^{6}Li	^{12}C	5.92	4.5, 5.8, 6.4, 7.5, 9, 11, and 13	[26]
^{6}Li	^{27}Al	8.91	7, 8, 10, 12, 18, and 34	[27,28]
^{6}Li	^{28}Si	9.46	7.5, 9, 11, 13, 16, 20, 21, 25, 34, 60, 75, 90, 210, and 318	[29–35]
^{6}Li	^{58}Ni	14.67	9.9, 11.2, 12.1, 13, and 14	[36]
^{6}Li	^{59}Co	14.07	12, 18, 26, and 30	[37]
^{6}Li	^{64}Zn	15.23	11.8, 12.8, 13.6, 14.8, 16.3, 17.8, 19.8, and 21.9	[38]
^{6}Li	^{90}Zn	18.29	14.9, 16.9, 18.9, 20.9, 24.9, and 29.9	[39]
^{6}Li	^{112}Sn	21.43	21, 22, 23, 30, and 35	[40,41]
^{6}Li	^{116}Sn	21.21	20, 22, 23, 26, 30, and 35	[40]
^{6}Li	^{120}Sn	21.02	19, 24, 27, and 30	[42,43]
^{6}Li	^{208}Pb	29.42	23, 30, 36, 42, and 48	[44]
^{6}Li	^{209}Bi	29.74	24, 26, 28, 30, 32, 32.8, 34, 36, 38, 40, 44, and 50	[45]
^{7}Li	^{12}C	6.10	4.5, 5.8, 9, 11, and 13	[26]
^{7}Li	^{27}Al	9.00	7, 8, 9, 10, 11, 12, 13, 14, 16, 18, and 19	[46–49]
^{7}Li	^{28}Si	9.55	8, 8.5, 9, 10, 11, 13, 15, 16, 21, 26, 36, and 350	[29,50–52]
^{7}Li	^{59}Co	14.05	12, 18, 26, and 30	[53]
^{7}Li	^{64}Zn	15.20	13, 13.8, 15, 16.6, 18.3, and 20.4	[54]
^{7}Li	^{116}Sn	21.08	18, 19, 20, 21, 22, 23, 24, 26, 28, 30, and 35	[55,56]
^{7}Li	^{120}Sn	20.87	20, 22, 24, 26, 28, and 30	[15,57]
^{7}Li	^{138}Ba	22.44	21, 22, 23, 24, 28, 30, and 32	[58]

that describes these points well but does not describe the overall angular distribution (especially in the backward region). In these cases, we slightly modified the depth to obtain the best visual fit. We needed to make such modifications in eight of the angular distributions of ^{6}Li projectile and in seven of the elastic angular distributions of ^{7}Li projectile, which represent around 10% of the total number of data sets used.

With the final values that led to the best fits of the studied angular distributions, the next step consisted of studying the dependence of these values as a function of the bombarding energies of the projectiles. Since the different systems have different Coulomb barrier energies (as can be seen from Table I), the best way to compare them is to display the reaction energy as a function of the Coulomb barrier, where values less than 1 represent bombarding energies below the barrier and values greater than 1 indicate reactions occurring at energies above the barrier. To this end, we now introduce the variable E_R, given by

$$E_R = \frac{E_{\text{lab}}}{E_{\text{lab}}^{\text{barr}}}, \qquad (3)$$

In Eq. (3), $E_{\text{lab}}^{\text{barr}} = \left(\frac{0.9 Z_{\text{proj}} Z_{\text{targ}}}{A_{\text{proj}}^{1/3} + A_{\text{targ}}^{1/3}}\right) \cdot \left(\frac{A_{\text{proj}} + A_{\text{targ}}}{A_{\text{targ}}}\right)$ MeV is the Coulomb barrier expressed in the laboratory framework, and E_{lab} is the impinging energy of the projectile. Equation (3) allows the comparison among all the systems as they are now normalized by their own barrier. To obtain the behavior of the adjusted values and compare them to those obtained by the Cook potential, it seems is natural to define a variable W_{rat} as

$$W_{\text{rat}} = \frac{W_{\text{adj}}}{W_{\text{Cook}}}. \qquad (4)$$

In Eq. (4), W_{adj} is the depth of the adjusted imaginary potential obtained through the χ^2 minimization procedure,

while W_{Cook} is the depth of the imaginary optical potential obtained through the Cook systematics given in Eqs. (1) and (2). The variable W_{rat} is defined as the ratio between the best fit obtained with the adjusted values and the values expected by the Cook systematics. Therefore, any discrepancy between the Cook systematics and the depth necessary for the best fit can be visualized through a plot of W_{rat} as a function of E_R. This comparison is made for both projectiles in Fig. 1.

One may visualize in Fig. 1 that for bombarding energies below the region where $E_R \approx 2$, the W_{rat} value decreases
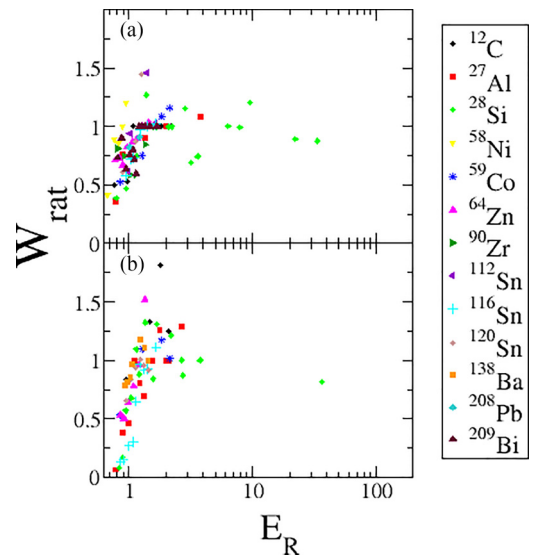

FIG. 1. W_{rat} in function of E_R for ^{6}Li (a) and ^{7}Li (b). The elastic scattering with different targets are associated to a shape and color code displayed in the figure.

rapidly (associated to the fact that the usual Cook systematics gives a very absorptive potential), indicating a need to reduce the depth of the potential below this energy region. In fact, the decrease is so fast that we have opted do display Fig. 1 in a logarithmic scale on the horizontal axis for a better visualization. The oscillations observed as the reaction energies increase are not a big problem since the Cook potential has already been proven to work well in this region in previous works, besides that, further calculations show that the obtained elastic angular distributions are not significantly affected by using the best fit depth or the one obtained from Cook systematics. It is desirable that the obtained correction to Cook systematics replicates the depths of Eqs. (1) and (2) in this energy region. Observing Fig. 1 one will notice that the amount of data points in the region $E_R > 5$ is much smaller than the region below and around the Coulomb barrier. This is not a problem for the results here obtained since this high energy region has been already well studied in the original work of [14] and the results there obtained have been used and proved themselves consistent since then. We would like to stress once more that the main focus of the present work is in the region around and below the Coulomb barrier, so it is natural that more data points for this specific region will be adopted, besides it, one also should notice that, until this point, the behavior presented (fast decay followed by a plateau) in Fig. 1 comes exclusively from the data points themselves, this way, the correction presented in the next section aims merely to reproduce such behavior.

III. ENERGY CORRECTION TO COOK POTENTIAL

The final optical potential that best describes the elastic scattering data of ^{6,7}Li projectiles should be both mass and energy dependent. While the Cook potential captures the A dependence, the energy dependence can be incorporated by adding a multiplicative modulation factor to the $W_{\mathrm{Cook}}(A)$ imaginary depth calculated from Eqs. (1) and (2). The energy-dependent factor can be obtained from the behavior seen in Fig. 1, and therefore, it will vary as a function of $E_R(E_{\mathrm{lab}})$. Thus, the final corrected imaginary potential (denoted as W_{corr} henceforth) should be consistent with the form

$$W_{\mathrm{corr}}(E_{\mathrm{lab}}, A) = F(E_R) \cdot W_{\mathrm{Cook}}(A). \qquad (5)$$

Equation (50 provides the final form of the corrected $W_{\mathrm{corr}}(E_{\mathrm{lab}}, A)$ potential. The modulation function $F(E_R)$ is energy-dependent and E_R can be obtained from Eq. (3). The explicit form of $F(E_R)$ will now be determined from the best fits to the data in Fig. 1. It is important to remember that this function should exhibit a rapid decay as E_R approaches the Coulomb barrier, and then converge to a plateau close to unity for energies above it. These features can be expressed mathematically as $F(E_R) \rightarrow 1$ and $W_{\mathrm{corr}}(E_{\mathrm{lab}}, A) \rightarrow W_{\mathrm{Cook}}(A)$.

The first step in the analysis was to determine the appropriate shape for the $F(E_R)$ function. It must satisfy two conditions: it should converge to one as E_R increases and have a rapid decline at low E_R values. An exponential function seems a natural choice for this rapid decline. However, the problem with using a pure exponential function is that it would vanish for high E_R values, leaving no imaginary potential,
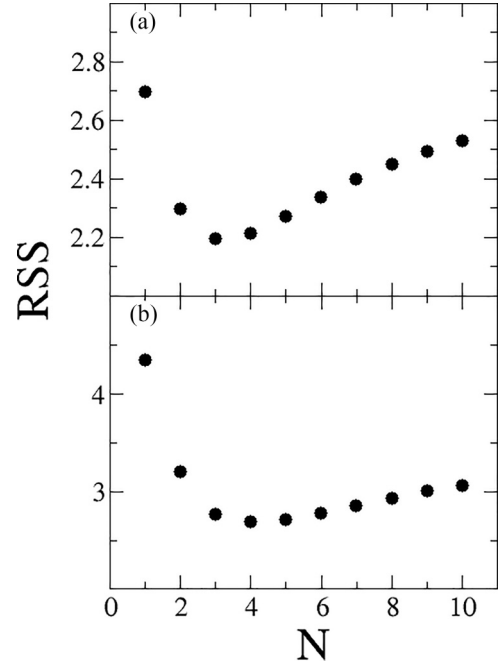

FIG. 2. The RSS of Eq. (6) adjusted to the experimental data as a function of the N integer value for ^{6}Li (a) and ^{7}Li (b).

which has no physical meaning. To avoid this, a constant term is added to the final form of the $F(E_R)$ function. An attempt to capture these features was made by proposing the form shown in Eq. (6):

$$F(E_R) = A_1 + A_2 \cdot e^{-(E_R)^N}. \qquad (6)$$

In Eq. (6), A_1 and A_2 are adjustable parameters, and N is an integer number that will be varied to obtain the best fit to the data. Other forms of Eq. (6), with more adjustable parameters, have been tested but resulted in worse adjustments to the data. Examples of these tentative functions include $F(E_R) = A_1 + e^{\frac{A_2}{E_R^{A_3}}}$ and $F(E_R) = A_1 + A_2 \cdot e^{\frac{A_3}{E_R^N}}$, among others. Therefore, the simpler form of Eq. (6) was kept, and the value of the N integer parameter was studied. Another advantage of this form is that Eq. (6) is linear in the adjustable parameters A_1 and A_2, which helps to guarantee that the general minimum value of the parameters is obtained when performing the minimum square method. In order to maintain the linearity of the $F(E_R)$ function, the N parameter in Eq. (6) was kept as an integer, instead of allowing it to be adjusted as a real number. The best fit for the integer value of N for each lithium isotope was obtained by studying the variation of the residual sum of squares (RSS) of each fit as a function of the N parameter. This study is shown in Fig. 2.

The RSS is defined as RSS $= \sum (W_{\mathrm{rat}}^{\mathrm{exp}} - F(E_R))^2$, which gives a measure of the discrepancy between the experimental $W_{\mathrm{rat}}^{\mathrm{exp}}$ values and the N-dependent $F(E_R)$ estimation from the model. The function that best fits the data is the one with the lowest RSS value. In this study, $N = 3$ was obtained for ^{6}Li projectile, while $N = 4$ was obtained for ^{7}Li. The values for A_1 and A_2 parameters that give the best fit to data are shown

TABLE II. Table showing the best fits obtained from Eq. (6) for each projectile. The adopted N integer values were extracted from Fig. 2. The A_1 and A_2 parameters are those of Eq. (6).

Projectile	N	A_1	A_2
^{6}Li	3	1.021(27)	−0.659(85)
^{7}Li	4	1.116(36)	−1.35(13)

in Table II, while the adjusted functions for each projectile can be visualized in Fig. 3 (solid red lines) compared to the experimental data (black circles). The form of Eq. (6) is used instead of a linear polynomial form due to its simplicity regarding the low number of adjustable parameters. If one desires to use a polynomial form, one should make the adjustment using a high-order polynomial, which implies a large number of variables to be adjusted. For example, in the ^{6}Li case, a polynomial of order 6 (composed of seven adjustable parameters) should be implemented if one desires to have a similar RSS value when compared to the form of Eq. (6).

From Fig. 3, it is observed that the proposed function fits the experimental data well, displaying a rapid fall for W_{rat} at low E_R values and converging to one as E_R becomes larger. In other words, the final potential converges to the Cook potential for higher reaction energies. One should note that the shape adopted in Eq. (6) with the parameters displayed in Table II could imply negative values for the $F(E_R)$ function for low values of E_R, which has no physical meaning. One should keep in mind that the present correction for the Cook potential is obtained based on the available data present in
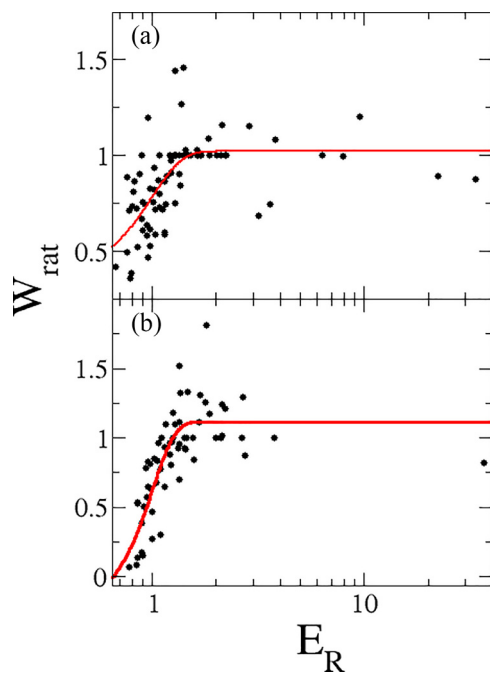
the literature, which mainly covers the region over $E_R > 0.7$. Thus, more data are needed to obtain a more general function to study other regions of the function. The results obtained here should be used in the region over $E_R \approx 0.7$. Even though the scattering at low energies is expected to be essentially Rutherford, a small contribution to the imaginary potential is expected since some dissipative processes still may occur (like the complete and incomplete fusion) even with lower probability.

One may argue that introducing a variation in the imaginary potential implies that variations in the real part of the optical potential should also be introduced. Effects like the break-up threshold anomaly [59] have already demonstrated that such dependence could occur. However, the amount of available data in the literature and the reaction energy at which they have been measured do not allow us to perform such a study. In Ref. [59], the break-up threshold anomaly has been studied in the ^{6}Li + ^{208}Pb reaction, and the results show that for the $E_R > 0.7$ region, a minor alteration in the real part of the potential was necessary. The data used in the present analysis are for this same energy range; thus, it is expected that no modifications in the real potential are necessary for the present work.

To summarize, in order to obtain the corrected potential, one needs to follow the routine: (1) obtain the original Cook potential using Eqs. (1) or (2); (2) calculate the E_R value, using Eq. (3) and the $E_{\mathrm{lab}}^{\mathrm{barr}}$ discussed in the text; (3) calculate the $F(E_R)$ function (adopting the parameters of Table II); and (4) obtain the final optical potential via Eq. (5). In the next section, a comparison of this new optical potential with some of the existing potentials in literature is presented.

A. Comparison with other optical potentials

In this section, the elastic scattering calculations obtained with the new energy-corrected optical potential proposed in this work are compared with those obtained with the original Cook potential of Ref. [14] and with the optical potentials proposed by Xu *et al.* of Refs. [12,13]. Such comparisons are the main aim of this section. Figures 4–7 bring the comparison of the elastic scattering data for several systems with the optical model calculations using the Cook potential (solid blue line), the energy-corrected potential presented in this work (dashed red line), and the potentials proposed by Xu *et al.* (dotted green line). The figures tried to display the comparisons comprising different mass numbers of the targets, as also different bombarding energies relatively to the barrier, this way, each system is analyzed in two different energies, one below ($E_R < 1$) and one above ($E_R > 1$) the barrier, whenever possible.

Figures 4 and 5 show a comparison of the three theoretical calculations described before with experimental data for the ^{6}Li projectile. The panels on the left side of the figures display the comparison of calculations to experimental data for ^{27}Al, ^{28}Si, ^{58}Ni, ^{64}Zn, ^{90}Zr, ^{112}Sn, ^{116}Sn, ^{120}Sn, and ^{209}Bi targets with bombarding energies below their respective Coulomb barriers. On the right side of Fig. 5, the same comparison is made for energies above (or close to) the barrier. An overall analysis of both figures indicates that the energy-dependent
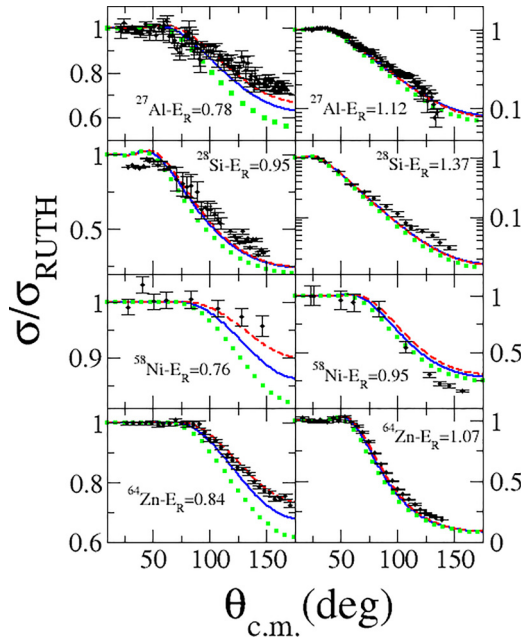

FIG. 3. W_{rat} in function of E_R for ^{6}Li (a) and ^{7}Li (b). The black circles are the experimental data for all targets and the solid red lines display the best fit of Eq. (6) using the parameters shown in Table II.

FIG. 4. Elastic angular distribution of ^{6}Li projectile with ^{27}Al ($E = 7$ and 10 MeV), ^{28}Si ($E = 9$ and 13 MeV), ^{58}Ni ($E = 11.2$ and 14 MeV), and ^{64}Zn ($E = 12.8$ and 16.3 MeV) targets. The solid blue line brings the Cook theoretical calculations, the dashed red line brings the results calculated with the optical potential proposed in this work, while the dotted green line brings the results obtained with the potential proposed in Ref. [12]. The horizontal scale is the same for all the panels. The vertical scales of the left panels are shown to the left of them, while the scale values for the right panels are shown in the right side of them.

FIG. 5. Elastic angular distribution of ^{6}Li projectile with ^{90}Zr ($E = 14.9$ and 24.9 MeV), ^{112}Sn ($E = 21$ and 35 MeV), ^{116}Sn ($E = 20$ and 35 MeV), ^{120}Sn ($E = 19$ and 27 MeV), and ^{209}Bi ($E = 24$ and 36 MeV) targets. The solid blue line brings the Cook theoretical calculations, the dashed red line brings the results calculated with the optical potential proposed in this work, while the dotted green line brings the results obtained with the potential proposed in Ref. [12]. The horizontal scale is the same for all the panels. The vertical scales of the left panels are shown to the left of them, while the scale values for the right panels are shown in the right side of them.

Cook potential proposed in this work provides better results for reactions occurring below the Coulomb barrier ($E_R < 1$). Particularly, for the ^{27}Al, ^{58}Ni, ^{64}Zn, ^{112}Sn, ^{116}Sn, and ^{120}Sn systems, the new potential provides a better description of experimental data below the barrier when compared to the one proposed by Xu *et al.* and the original Cook potential. From both figures, it can also be observed from the right panels of both figures that the new potential rapidly converges to the results obtained with the original Cook potential, as desired when the form of Eq. (6) was proposed. Regarding energies above the barrier, some systems show that the new and the original Cook potential have a better agreement with data (i.e., ^{27}Al and ^{64}Zn), while for the ^{58}Ni, ^{120}Sn, and ^{209}Bi systems, the potential proposed in Ref. [12] provides a better agreement. One should notice that the small sample of systems analyzed in the present work (when compared to the literature) does not allow one to point if there is a particular potential that is superior to the others in describing the elastic scattering of systems involving the ^{6}Li projectile. To give a quantitative answer, one needs to make a comprehensive study including the maximum number of systems available in the literature, over a vast energy range. This is clearly not the aim of the present work and will not be done. However, from the analysis of the systems displayed in Figs. 4 and 5, we have an indication that the energy correction to the Cook potential
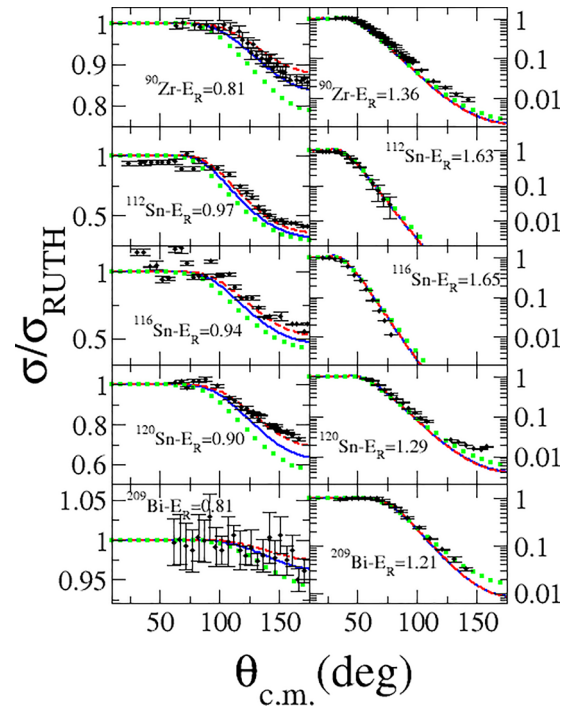
provides a better description of data at energies below the Coulomb barrier.

The overall effect of the new optical potential (when compared to the one originally proposed by Cook) consists in enhancement of the elastic angular distribution for the bombarding projectile energies below the Coulomb barrier. It occurs because the multiplicative $F(E_R)$ function gives a number smaller than 1 in this energy range, causing the decrease of the imaginary potential depth. A possible qualitative explanation for the necessity of decreasing the magnitude of the imaginary potential depth lies in the fact that, for energies below the barrier, the reduction of the number of reaction channels is expected.

Figures 6 and 7 show a comparison between the three theoretical calculations described earlier and experimental data for ^{7}Li projectiles. The figures display elastic angular distributions for reactions with ^{12}C, ^{27}Al, ^{28}Si, ^{59}Co, ^{64}Zn, ^{116}Sn, ^{120}Sn, and ^{138}Ba targets. Similar conclusions can be drawn for the ^{7}Li isotope as were obtained for ^{6}Li. Once again, for energies below the Coulomb barrier, the new proposed potential tends to give a better description of experimental data, especially for ^{27}Al, ^{28}Si, ^{59}Co, ^{64}Zn, ^{116}Sn, and ^{120}Sn targets. The main difference observed for the ^{7}Li projectile (compared
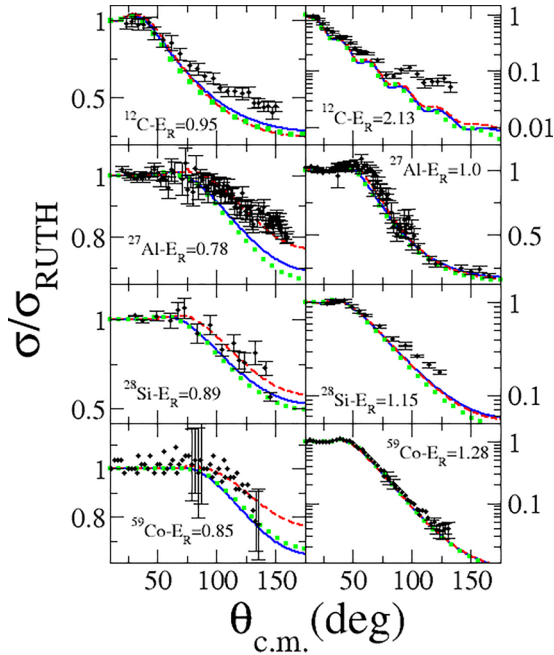
FIG. 6. Elastic angular distribution of ^{7}Li projectile with ^{12}C ($E = 5.8$ and 13 MeV), ^{27}Al ($E = 7$ and 9 MeV), ^{28}Si ($E = 8.5$ and 11 MeV), and ^{59}Co ($E = 12$ and 18 MeV) targets. The solid blue line brings the Cook theoretical calculations, the dashed red line brings the results calculated with the optical potential proposed in this work, while the dotted green line brings the results obtained with the potential proposed in Ref. [13]. The horizontal scale is the same for all the panels. The vertical scales of the left panels are shown to the left of them, while the scale values for the right panels are shown in the right side of them.

FIG. 7. Elastic angular distribution of ^{7}Li projectile with ^{64}Zn ($E = 15$ and 18.3 MeV), ^{116}Sn ($E = 18$ and 23 MeV), ^{120}Sn ($E = 20$ and 24 MeV), and ^{138}Ba ($E = 22$ and 30 MeV). The solid blue line brings the Cook theoretical calculations, the dashed red line brings the results calculated with the optical potential proposed in this work, while the dotted green line brings the results obtained with the potential proposed in Ref. [13]. The horizontal scale is the same for all the panels. The vertical scales of the left panels are shown to the left of them, while the scale values for the right panels are shown in the right side of them.

to ^{6}Li) is that the three calculations here performed appear to give very similar results for energies above the Coulomb barrier. Although a quantitative comparison of the potentials and how they fit experimental data would yield more conclusive results, the analysis of Figs. 6 and 7 indicates that the new energy-dependent potential proposed in this work provides a better description of data in the energy region below the Coulomb barrier.

When one is dealing with the ^{7}Li projectile, besides the possibility of the break up for this isotope it is also observed that such nucleus has an excited state with a reasonably low excitation energy, which usually has an important role in the correct description of the reaction mechanisms (as discussed in [15]). The $3/2^{-}$ ground state (g.s.) is separated from the $1/2^{-}$ excited state just by 477 keV, this way, such channel may be easily acquired when one performs nuclear reaction experiments. Typically, one couples the inelastic excitation of projectile/target to the coupling scheme and uses the Cook potential as the optical potential. This procedure is correct when the existing coupling between the elastic and inelastic channels is negligible, which is usually true concerning to the inclusion of inelastic states of target, however, the inclusion of the $1/2^{-}$ excited state ^{7}Li typically has a great impact in calculations, this way, it is expected that the use of the original optical potential will cause a double counting, turning data
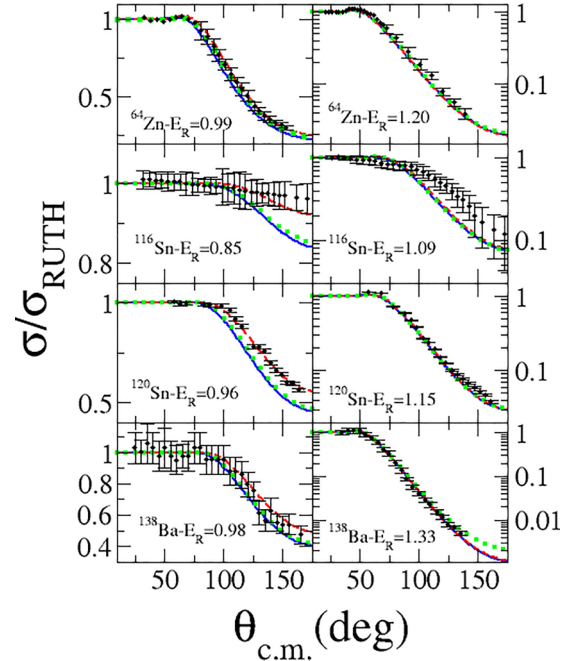
and calculations incompatible to each other. As the g.s. of the ^{7}Li projectile has a large spin and the nucleus presents a high static quadrupole moment, it is also expected that the reorientation effect [60–62] of the g.s. could contribute to the correct theoretical description of the elastic scattering angular distribution. This way, even that the present work furnishes a good description for elastic data below the Coulomb barrier, if one wants to perform theoretical calculations explicitly including the reorientation effect of the g.s. and the first excited state of ^{7}Li projectile, modifications in the optical potential adopted must be performed.

B. Corrected potential used in a transfer case

Up until this point, we have mainly focused on how the correct choice of potential reflects on the elastic channel of any given reaction. As is well known, the elastic channel usually is the one which more influences the remaining processes, this way, the correct description of it may affect all the remaining reaction channels. In order to verify this point, we performed coupled reaction channel (CRC) calculations to explore the influence that an optical potential may present in the other reaction channels. We used the one-neutron stripping data of the ^{7}Li + ^{120}Sn → ^{6}Li + ^{121}Sn reaction at 20 MeV from Ref. [15]. The experimental data consist of the
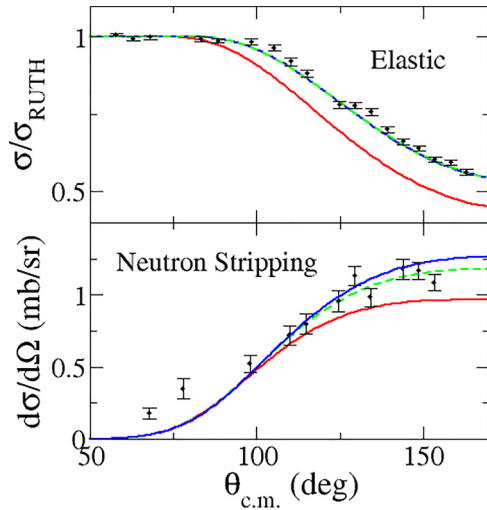
FIG. 8. The upper panel represents the elastic data of ^{7}Li $+ ^{120}$Sn reaction with bombarding energy of 20 MeV being compared to CRC calculations using the original Cook potential (solid red line) and the modified Cook potential proposed by this work modifying just the entrance partition (dashed green line) as well as both partitions (solid blue line). The lower panel displays the same calculations compared to one neutron stripping transfer channel (^{6}Li $+ ^{121}$Sn). The transfer data (as also the displayed curves) are composed by the sum of three low-lying states of ^{121}Sn ($3/2^+$ g.s., $11/2^-$ at 0.006 MeV, and $1/2^+$ with 0.060 MeV), since they could not be experimentally distinguished.

sum of three low-lying states of ^{121}Sn ($3/2^+$ ground state, $11/2^-$ at 0.006 MeV, and $1/2^+$ with 0.060 MeV). The CRC calculations included only the elastic channel in the entrance partition and the aforementioned states of the final partition. The optical potentials included in the initial and final partitions were the Cook potential with no corrections (displayed in Fig. 8 as the solid red line), as well as the Cook potential with the $F(E_R)$ function using parameters from Table II of the present work to correct only the entrance partition (dashed green line), as well as the entrance and the final partition (solid blue line). The spectroscopic information required to describe the one-neutron transfer was the same as that used in the original work [15] (Table II). The CRC calculations were performed using prior representation with a complex remnant. The valence neutron interaction with both cores was described by a real Woods-Saxon potential (reduced radius $r_o =$ 1.25 fm and diffuseness $a = 0.75$ fm), whose depth was adjusted to reproduce the neutron-core binding energy. A spin-orbit interaction with similar parameters was also included.

From the upper panel of Fig. 8, one may observe the already discussed importance of adopting the corrected Cook potential and how it affects the proper description of elastic data. Since there is almost no difference between the calculations including the correction just in the entrance partition (dashed green line) from that including it in both of them (solid blue line), one may argue that the elastic channel is sensible mainly to the first optical potential. The lower panel shows the importance of also adopting such correction of the optical potential on other reaction channels. One may

observe that the use of a mistaken potential may has some influence directly in the proper description of the transfer processes, where the corrected potential describes the one neutron transfer data better than the noncorrected potential, which clearly tends to underestimate the transfer cross sections. The observed difference between the solid red line and the dashed green line shows once again the importance of properly describing the elastic channel and how it affects the transfer reaction. The solid blue line shows that the proper description of the final partition optical potential also plays a relevant role in the transfer reaction.

This example illustrates how the use of an incorrect potential could lead to erroneous conclusions about the obtained spectroscopic information. As discussed in Ref. [63], similar results can be obtained by changing other spectroscopic parameters, such as the nuclear radius adopted or the theoretically calculated spectroscopic amplitudes. Therefore, this result emphasizes the importance of choosing the appropriate optical potential.

IV. CONCLUSIONS

The present work has made an extensive study of the available data on literature in order to study a possible dependence on energy of the Cook potential for ^{6,7}Li projectiles. The original Cook potential has adjusted the parameters of two WS potentials (one real and the other imaginary) to the experimental data. Originally, five of these parameters have been kept constant, finding a dependence of the imaginary potential depth with the target mass. The present work proposed to correct such depth by a function $F(E_R)$, which depends on the bombarding energy of the projectile. After selecting the available data in a large reaction energy range, the best fit to the elastic scattering has been obtained by the use of a minimization χ^2 routine (SFRESCO code) in which the imaginary potential depth was the only parameter allowed to be varied. The ratio of the best fitted depth with the original value proposed by the Cook potential has been shown in function of a E_R parameter, which is the ratio of the projectile bombarding energy to the Coulomb barrier of each system. This indicated a modulation function to the imaginary potential depth, whose typical behavior consisted in a rapid rise for the region $E_R <$ 1, followed by a plateau which tends to original Cook original potential.

The comparison of the results obtained with the new energy dependent optical potential proposed in this work with those obtained using the original Cook potential and the ones proposed by Xu $et\ al.$ in Refs. [12,13] indicates that this new potential furnishes a better description of experimental data in the energy range of bombarding energies below the Coulomb barrier compared to the others. In the energy range above the Coulomb barrier, it seems that the optical potential proposed by Ref. [12] gives a better description of data of ^{6}Li projectile, while all the potentials give similar results for reactions involving ^{7}Li projectile.

Finally, the last section of this work shows how the correct choice of the adopted optical potential is mandatory even when one desires to study other channels than not the elastic itself. One example of the ^{7}Li $+ ^{120}$Sn $\rightarrow ^6$Li $+ ^{121}$Sn

transfer reaction (with bombarding energy of 20 MeV) has been shown and the wrong description of the optical potential resulted in an underestimation of the one neutron stripping cross sections. Such error in this description could lead to errors of the interpretation of data, as also of the spectroscopic information contained in them.

ACKNOWLEDGMENTS

[1] B. D. Fields, Annu. Rev. Nucl. Part. Sci. **61**, 47 (2011).

[2] M. Dasgupta, D. J. Hinde, K. Hagino, S. B. Moraes, P. R. S. Gomes, R. M. Anjos, R. D. Butt, A. C. Berriman, N. Carlin, C. R. Morton *et al.*, Phys. Rev. C **66**, 041602(R) (2002).

[3] C. L. Guo, G. L. Zhang, S. P. Hu, J. C. Yang, H. Q. Zhang, P. R. S. Gomes, J. Lubian, X. G. Wu, J. Zhong, C. Y. He *et al.*, Phys. Rev. C **92**, 014615 (2015).

[4] H. Rawitscher, Phys. Rev. C **9**, 2210 (1974).

[5] M. Yahiro, N. Nakano, Y. Iseri, and M. Kamimura, Prog. Theor. Phys. **67**, 1467 (1982).

[6] M. Yahiro, N. Nakano, Y. Iseri, and M. Kamimura, Prog. Theor. Phys. Suppl. **89**, 32 (1986).

[7] N. Austern, Y. Iseri, M. Kamimura, M. Kawai, G. Rawitscher, and M. Yahiro, Phys. Rep. **154**, 125 (1987).

[8] Y. Sakuragi, Phys. Rev. C **35**, 2161 (1987).

[9] J. A. Tostevin, S. Rugmai, and R. C. Johnson, Phys. Rev. C **57**, 3225 (1998).

[10] E. O. Alt, P. Grassberger, and W. Sandhas, Nucl. Phys. B **2**, 167 (1967).

[11] J. Rangel, M. R. Cortes, J. Lubian, and L. F. Canto, Phys. Lett. B **803**, 135337 (2020).

[12] Y. Xu, Y. Han, J. Hu, H. Liang, Z. Wu, H. Guo, and C. Cai, Phys. Rev. C **97**, 014615 (2018).

[13] Y. Xu, Y. Han, J. Hu, H. Liang, Z. Wu, H. Guo, and C. Cai, Phys. Rev. C **98**, 024619 (2018).

[14] J. Cook, Nucl. Phys. A **388**, 153 (1982).

[15] V. A. B. Zagatto, J. Lubian, L. R. Gasques, M. A. G. Alvarez, L. C. Chamon, J. R. B. Oliveira, J. A. Alcantara-Nunez, N. H. Medina, V. Scarduelli, A. Freitas, I. Padron, E. S. Rossi, Jr., and J. M. B. Shorto, Phys. Rev. C **95**, 064614 (2017).

[16] A. H. Amer and Y. E. Penionzhkevich, Nucl. Phys. A **1015**, 122300 (2021).

[17] M. Gómez-Ramos, and A. M. Moro, Phys. Rev. C **95**, 034609 (2017).

[18] E. Muskat, J. Carter, R. Fearick, and V. Hnizdo, Nucl. Phys. A **581**, 42 (1995).

[19] B. Mukeru, J. Lubian, and L. Tomio, Phys. Rev. C **105**, 024603 (2022).

[20] V. V. Pakar, A. Parmar, M. Prasanna, V. Jha, and S. Kailas, Phys. Rev. C **104**, 054603 (2021).

[21] J. A. Lei and A. M. Moro, Phys. Rev. Lett. **123**, 232501 (2019).

[22] S. K. Pandit, A. Shrivastava, K. Mahata, N. Keeley, V. V. Parkar, R. Palit, P. C. Rout, K. Ramachandran, A. Kumar *et al.*, Phys. Lett. B **820**, 136570 (2021).

[23] https://www-nds.iaea.org/exfor/

[24] S. M. Wong, *Introductory Nuclear Physics* (John Wiley & Sons, New York, 1998).

[25] I. J. Thompson, Comput. Phys. Rep. **7**, 167 (1988).

[26] J. E. Poling, E. Norbeck, and R. R. Carlson, Phys. Rev. C **5**, 1819 (1972).

[27] J. M. Figueira, J. O. Fernandez Niello, D. Abriola, A. Arazi, O. A. Capurro, E. de Barbara, G. V. Marti, D. Martinez Heimann, A. E. Negri, A. J. Pacheco, I. Padron, P. R. S. Gomes, J. Lubian, T. Correa, and B. Paes, Phys. Rev. C **75**, 017602 (2007).

[28] G. Ciangaru, R. L. McGrath, and F. E. Cecil, Nucl. Phys. A **380**, 147 (1982).

[29] M. Sinha, S. Roy, P. Basu, H. Majumdar, S. Santra, V. V. Parkar, K. S. Golda, and S. Kailas, EPJ Web Confer. **17**, 03004 (2011).

[30] A. Pakou, N. Alamanos, A. Lagoyannisa, A. Gillibert, E. C. Pollacco, P. A. Assimakopoulos, G. Doukelis, K. G. Ioannides, D. Karadimos, D. Karamanis, M. Kokkoris, E. Kossionides, N. G. Nicolis, C. Papachristodoulou, N. Patronis, G. Perdikakis, and D. Pierroutsakou, Phys. Lett. B **556**, 21 (2003).

[31] M. F. Vineyard, J. Cook, and K. W. Kemper, Nucl. Phys. A **405**, 429 (1983).

[32] M. Hugi, J. Lang, R. Mueller, E. Ungricht, K. Bodek, L. Jarczyk, B. Kamys, A. Magiera, A. Strzalkowski, and G. Willim, Nucl. Phys. A **368**, 173 (1981).

[33] Yu. A. Glukhov, A. S. Demyanova, S. I. Drozdov, M. V. Zhukov, V. I. Manko, B. G. Novatsky, A. A. Ogloblin, S. B. Sakuta, D. N. Stepanov, and L. V. Chulkov, Yader. Fiz. **34**, 312 (1981).

[34] A. Nadasen, T. Stevens, J. Farhat, J. Brusoe, P. Schwandt, J. S. Winfield, G. Yoo, N. Anantaraman, F. D. Becchetti, J. Brown, B. Hotz, J. W. Janecke, D. Roberts, and R. E. Warner, Phys. Rev. C **47**, 674 (1993).

[35] A. Nadasen, M. McMaster, M. Fingal, J. Tavormina, P. Schwandt, J. S. Winfield, M. F. Mohar, F. D. Becchetti, J. W. Janecke, and R. E. Warner, Phys. Rev. C **39**, 536 (1989).

[36] E. F. Aguilera, E. Martinez-Quiroz, D. Lizcano, A. Gómez-Camacho, J. J. Kolata, L. O. Lamm, V. Guimarães, R. Lichtenthäler, O. Camargo, F. D. Becchetti, H. Jiang, P. A. DeYoung, P. J. Mears, and T. L. Belyaeva, Phys. Rev. C **79**, 021601(R) (2009).

[37] C. Beck, N. Rowley, M. Rousseau, F. Haas, P. Bednarczyk, S. Courtin, N. Kintz, F. Hoellinger, P. Papka, S. Szilner *et al.*, arXiv:nucl-ex/0411002 (2004).

[38] M. Zadro, P. Figuera, A. Di Pietro, M. Amorini, M. Fisichella, O. Goryunov, M. Lattuada, C. Maiolino, A. Musumarra, V. Ostashko, M. Papa, M. G. Pellegriti, F. Rizzo, D. Santonocito, V. Scuderi, and D. Torresi, Phys. Rev. C **80**, 064610 (2009).

[39] H. Kumawat, V. Jha, B. J. Roy, V. V. Parkar, S. Santra, V. Kumar, D. Dutta, P. Shukla, L. M. Pant, A. K. Mohanty, R. K. Choudhury, and S. Kailas, Phys. Rev. C **78**, 044617 (2008).

[40] N. N. Deshmukh, S. Mukherjee, D. Patel, N. L. Singh, P. K. Rath, B. K. Nayak, D. C. Biswas, S. Santra, E. T. Mirgule, L. S. Danu, Y. K. Gupta, A. Saxena, R. K. Choudhury, R. Kumar, J. Lubian, C. C. Lopes, E. N. Cardozo, and P. R. S. Gomes, Phys. Rev. C **83**, 024607 (2011).

[41] D. Chattopadhyay, S. Santra, A. Pal, A. Kundu, K. Ramachandran, R. Tripathi, D. Sarkar, S. Sodaye, B. K. Nayak, A. Saxena, and S. Kailas, Phys. Rev. C **94**, 061602(R) (2016).

[42] V. A. B. Zagatto, M. Gómez-Ramos, L. R. Gasques, A. M. Moro, L. C. Chamon, M. A. G. Alvarez, V. Scarduelli, J. P. Fernández-Garcia, J. R. B. de Oliveira, A. Lépine-Szily, and A. Arazi, Phys. Rev. C **106**, 014622 (2022).

[43] V. V. Davydov, B. G. Novashkii, A. A. Ogloblin, S. B. Sakuta, D. N. Stepanov, and V. I. Chuev, Ross. Aka. Nau. **35**, 2399 (1971).

[44] H. Gemmeke, B. Deluigi, L. Lassen, and D. Scholz, Z. Phys. A **286**, 73 (1978).

[45] S. Santra, S. Kailas, K. Ramachandran, V. V. Parkar, V. Jha, B. J. Roy, and P. Shukla, Phys. Rev. C **83**, 034616 (2011).

[46] J. Lubian, T. Correa, B. Paes, J. M. Figueira, D. Abriola, J. O. Fernandez Niello, A. Arazi, O. A. Capurro, E. De Barbara, G. V. Marti, D. Martinez Heinmann, A. E. Negri, A. J. Pacheco, I. Padron, and P. R. S. Gomes, Nucl. Phys. A **791**, 24 (2007).

[47] D. Patel, S. Santra, S. Mukherjee, B. K. Nayak, P. K. Rath, V. V. Parkar, and R. K. Choudhury, Pramana - J. Phys. **81**, 587 (2013).

[48] K. Kalita, S. Verma, R. Singh, J. J. Das, A. Jhingan, N. Madhavan, S. Nath, T. Varughese, P. Sugathan, V. V. Parkar, K. Mahata, K. Ramachandran, A. Shrivastava, A. Chatterjee, S. Kailas, S. Barua, P. Basu, H. Majumdar, M. Sinha, R. Bhattacharya *et al.*, Phys. Rev. C **73**, 024609 (2006).

[49] J. M. Figueira, D. Abriola, J. O. Fernandez Niello, A. Arazi, O. A. Capurro, E. De Barbara, G. V. Marti, D. Martinez-Heimann, A. J. Pacheco, J. E. Testoni, I. Padron, P. R. S. Gomes, and J. Lubian, Phys. Rev. C **73**, 054603 (2006).

[50] P. Schumacher, N. Ueta, H. H. Duhm, K.-L. Kubo, and W. J. Klages, Nucl. Phys. A **212**, 573 (1973).

[51] A. Pakou, N. Alamanos, G. Doukelis, A. Gillibert, G. Kalyva, M. Kokkoris, S. Kossionides, A. Lagoyannis, A. Musumarra, C. Papachristodoulou, N. Patronis, G. Perdikakis, D. Pierroutsakou, E. C. Pollacco, and K. Rusek, Phys. Rev. C **69**, 054602 (2004).

[52] A. Nadasen, J. Brusoe, J. Farhat, T. Stevens, J. Williams, L. Nieman, J. S. Winfield, R. E. Warner, F. D. Becchetti, J. W. Janecke, T. Annakkage, J. Bajema, D. Roberts, and H. S. Govinden, Phys. Rev. C **52**, 1894 (1995).

[53] F. A. Souza, L. A. S. Leal, N. Carlin, M. G. Munhoz, R. Liguori Neto, M. M. de Moura, A. A. P. Suaide, E. M. Szanto, A. Szanto de Toledo, and J. Takahashi, Phys. Rev. C **75**, 044601 (2007).

[54] J. P. Fernández-García, M. Zadro, A. Di Pietro, P. Figuera, M. Fisichella, O. Goryunov, M. Lattuada, C. Marchetta, A. M. Moro, A. Musumarra, V. Ostashko, M. G. Pellegriti, V. Scuderi, E. Strano, and D. Torresi, Phys. Rev. C **92**, 054602 (2015).

[55] A. Kundu, S. Santra, A. Pal, D. Chattopadhyay, R. Tripathi, B. J. Roy, T. N. Nag, B. K. Nayak, A. Saxena, and S. Kailas, Phys. Rev. C **99**, 034609 (2019).

[56] N. N. Deshmukh, S. Mukherjee, B. K. Nayak, D. C. Biswas, S. Santra, E. T. Mirgule, S. Appannababu, D. Patel, A. Saxena, R. K. Choudhury, J. Lubian, and P. R. S. Gomes, Eur. Phys. J. A **47**, 118 (2011).

[57] A. Kundu, S. Santra, A. Pal, D. Chattopadhyay, R. Tripathi, B. J. Roy, T. N. Nag, B. K. Nayak, A. Saxena, and S. Kailas, Phys. Rev. C **95**, 034615 (2017).

[58] A. M. M. Maciel, P. R. S. Gomes, J. Lubian, R. M. Anjos, R. Cabezas, G. M. Santos, C. Muri, S. B. Moraes, R. L. Neto, N. Added, N. C. Filho, and C. Tenreiro, Phys. Rev. C **59**, 2103 (1999).

[59] M. S. Hussein, P. R. S. Gomes, J. Lubian, and L. C. Chamon, Phys. Rev. C **76**, 019902(E) (2007).

[60] G. R. Satchler, Nucl. Phys. A **45**, 197 (1963).

[61] G. R. Satchler and C. B. Fulmer, Phys. Lett. B **50**, 309 (1974).

[62] S. E. Hicks and M. T. McEllistrem, Nucl. Phys. A **468**, 372 (1987).

[63] L. R. Gasques, A. S. Freitas, L. C. Chamon, J. R. B. Oliveira, N. H. Medina, V. Scarduelli, E. S. Rossi Jr., M. A. G. Alvarez, V. A. B. Zagatto, J. Lubian, G. P. A. Nobre, I. Padron, and B. V. Carlson, Phys. Rev. C **97**, 034629 (2018).